Surface and Bulk Composition, Structure, and Photocatalytic Activity of Phosphate-Modified TiO_2

László Körösi,[†] Szilvia Papp,[†] Imre Bertóti,[‡] and Imre Dékány*[,†,§]

Supramolecular and Nanostructured Materials Research Group of the Hungarian Academy of Sciences, University of Szeged, H-6720 Szeged, Aradi v. t. 1, Hungary,Institute of Materials and Environmental Chemistry, Chemical Research Center, Hungarian Academy of Sciences, H-1525 Budapest, Pusztaszeri út 59, and Department of Colloid Chemistry, University of Szeged, H-6720 Szeged, Aradi v. t. 1, Hungary

Received March 13, 2007

Phoshpate-modified titania (P−TiO_2) samples of varying phosphate contents were prepared by the sol−gel method, and the photocatalytic activity was tested in the gas-phase degradation of ethanol at room temperature. DRIFT, UV−vis−DR, N_2 adsorption, and XRD methods were used to characterize the structural properties of the P−TiO_2 samples. XPS, ICP-AES, and SAXS investigations were additionally performed to further clarify the structural changes of the TiO_2 sample due to phosphate modification. We showed that the phosphate ions reacted with the TiO_2 surface and that a new crystalline titanium phosphate phase appeared during the calcination process. It was found that the structural and optical properties of the titania samples are strongly influenced by their phosphate content. The photocatalytic activity of the P−TiO_2 was compared with that of Degussa P25 titanium dioxide by ethanol photooxidation in the gas phase. We have shown that total degradation of ethanol is significantly faster on P−TiO_2 samples with optimal phosphate content than it is on Degussa TiO_2. Phosphate groups bound to the surface of titania are responsible for the enhanced photo-oxidation observed on P−TiO_2 samples.

Introduction

Heterogeneous photocatalysis is a well-known environmentally friendly process to degrade or transform volatile organic compounds (VOCs). The most promising and therefore the most widely studied photocatalyst is titanium dioxide. Both of its crystal structures, anatase and rutile, are extensively used as photocatalysts. In most reactions, anatase exhibits higher photocatalytic activity,[1,2] which is probably due to its slightly higher Fermi level and its higher surface density of hydroxyl groups.[3,4] Attempts have been made to improve the photoactivity of titania both in the visible and the UV range. The methods used usually include various surface modifications. Several studies were devoted to anionic modifications of TiO_2, among which halogenide ions received special attention. Minero and co-workers investigated the effect of fluoride ions on the photocatalytic degradation of phenol in aqueous TiO_2 suspension[5,6]. They found that the degradation rate of phenol increases as a function of the fluoride concentration. Luo et al.[7] studied Br^- and Cl^- co-doped titanium dioxide in water splitting and found higher photocatalytic activity with respect to the commercial TiO_2 photocatalyst Degussa P-25. Sulfated titania also shows an enhanced photoactivity for several subtrates, such as hexane, methanol, benzene, and trichloroethylene.[8,9,10]

The phosphate modification of titania has been the subject of a considerably smaller number of studies, whose results are highly diverse from a photocatalytic point of view. The latter is probably due to differences in preparation techniques and the different phosphate contents. Colón et al.[11] used different oxoacids (nitric, sulfuric, and phosphoric acid) for modifying TiO_2. They found that the photoactivity strongly decreased after phosphoric acid treatment. The poor photocatalytic behavior is determined by the appearance of pyrophosphate-like species at the surface. In contrast, Yu et al.[12] found that photocatalytic activity of TiO_2 increased because of phosphate modification. The effect was explained by the increased band gap energy, large surface area, and the existence of Ti ions in tetrahedral coordination. In our previous study,[13] phosphate-modified titanium oxides were investigated, changing the P/Ti molar ratio systematically. We showed that the phenol degradation on titania strongly

* Corresponding author. E-mail: i.dekany@chem.u-szeged.hu.
† Supramolecular and Nanostructured Materials Research Group of the Hungarian Academy of Sciences, University of Szeged.
‡ Hungarian Academy of Sciences.
§ Department of Colloid Chemistry, University of Szeged.

(1) Linsbigler, A. L.; Lu, G. Q.; Yates, J. T., Jr. *Chem. Rev.* **1995**, *95*, 735.
(2) Tanaka, K.; Capule, M. F. V.; Hisanga, T. *Chem. Phys. Lett.* **1991**, *187*, 73.
(3) Bickley, R. I.; Gonzales-Carreno, T.; Lees, J. L.; Palmisano, L.; Tilley, R. J. D. *J. Solid State Chem.* **1991**, *92*, 178.
(4) Gerischer, H.; Heller, A. *J. Electrochem Soc.* **1992**, *139*, 113.
(5) Minero, C.; Mariella, G.; Mauriono, V.; Pelizzetti, E. *Langmuir* **2000**, *16*, 2636.
(6) Minero, C.; Mariella, G.; Mauriono, V.; Vione, D.; Pelizzetti, E. *Langmuir* **2000**, *16*, 8964.
(7) Luo, H.; Takata, T.; Lee, Y.; Zhao, J.; Domen, K.; Yan, Y. *Chem. Mater.* **2004**, *16*, 846.
(8) Deng, X.; Yue, Y.; Gao, Z. *Appl. Catal., B* **2002**, *39*, 135.
(9) Muggli, D. S.; Ding, L. *Appl. Catal., B* **2001**, *32*, 181.
(10) Gómez, R.; López T.; Ortiz-Islas, E.; Navarrete, J.; Sánchez, E.; Tzompantzi, F. *J. Mol. Catal. A: Chem.* **2003**, *193*, 217.
(11) Colón, G.; Sánchez-Espana, J. M.; Hidalgo, M. C.; Navío, J. A. *J. Photochem. Photobiol., A* **2006**, *179*, 20.
(12) Yu, J. C.; Zhang, L.; Zheng, Z.; Zhao, J. *Chem. Mater.* **2003**, *15*, 2280.
(13) Körösi, L.; Dékány, I. *Colloid Surf., A* **2006**, *280*, 146.

10.1021/cm070692r CCC: $37.00
Published on Web 08/15/2007

depended on phosphate content. First, it was higher on low phosphate content P−TiO_2 than on pure TiO_2. Increasing the phosphate content above an optimal value, however, decreased the phenol degradation.

In this work, we have further investigated the effect of phosphate modification and made a comparison with pure titanium dioxide. Phosphorus/titanium atomic ratio was studied by XPS and ICP-AES measurements. The structural changes of the samples were followed by XRD and SAXS measurements. We also report here on the effect of surface-bound phosphate on the rate of ethanol photooxidation.

Experimental Section

Sample Preparation. In the preparation of TiO_2 and P−TiO_2 by the sol−gel method, 14.8 mL of titanium(IV)−isopropoxide (Ti-$(OPr^i)_4$) (Fluka) was diluted with 30 mL of 2-propanol (Reanal, Hungary, analytical grade); 25 mL of deionized water was added dropwise to $Ti(OPr^i)_4$ solution during stirring. After the hydrolysis process, 200 mL of a phosphoric acid (analytical grade, Reanal, Hungary) solution of varying concentration (2.5, 12.6, or 25.2 mmol/L) was added to the resulting titania suspension to prepare TiO_2 samples of varying phosphate content, with P−TiO_2 atomic ratios of 0.01, 0.05, and 0.10, respectively. The prepared samples were denoted as P−TiO_2/0.01, P−TiO_2/0.05, P−TiO_2/0.10. Pure titania was prepared by adding only 200 mL of deionized water. The suspensions were stirred for 2 h, centrifuged at 3500 rpm, and dried at 100 °C. All samples were calcined at 300, 500, 700, and 900 °C for 3 h. The heating rate was 10 °C/min.

Removal of Phosphate from P−TiO_2 Samples. Two grams of sample P−TiO_2/0.05 was dispersed in 100 mL of 1 M $NaHCO_3$ solution, and the suspension was kept at 60 °C for 24 h under intensive stirring. The recooled suspension was centrifuged and the sediment was redispersed in 50 mL of 0.1 M HCl in order to remove residual hydrogen carbonate. The system was recentrifuged and the sediment was washed in distilled water until it was free of chloride.

Sample Characterization. The Ti and P content of the samples were determined by all-argon sequential (Jobin-Yvon 24, France) inductively coupled plasma atomic emission (ICP-AES) spectrometry. The intensity of the spectral lines of 213.62 (P I) and 337.28 (Ti II) nm were measured.

X-ray photoelectron spectra were recorded on a Kratos XSAM 800 spectrometer operated at fixed analyzer transmission mode using Mg $K\alpha_{1,2}$ (1253.6 eV) excitation. The pressure of the analysis chamber was lower than 1×10^{-7} Pa. Wide scan spectra were recorded in the 100−1300 eV kinetic energy range using an 80 eV pass energy with 0.5 eV steps and a 0.5 s dwell time. Photoelectron lines of the main constituent elements, O1s, Ti2p, C1s, and P2p, were recorded at 40 eV pass energy by 0.1 eV steps and a minimum 1 s dwell time. Charge-referencing of the spectra was made to the energy of the narrow Ti $2p_{3/2}$ line set at 459.0 eV B.E. (binding energy), in accordance with our earlier results[14,15] and well-accepted reference data. This is consistent with referencing to the C1s line of the hydrocarbon type adventitious carbon (present or build up at the surface of the samples during spectra acquisition) at 284.8 eV B.E. Peak area intensities were measured by the Vision 2 spectral acquisition and evaluation software after removal of the Shirley- or linear-type background. Quantitative analysis, i.e., the atomic concentration of the constituents, was performed by the XPS MultiQuant programs[16] using experimentally determined photoionization cross-sectional data of Evans et al.[17] and asymmetry parameters of Reilman et al.[18]

DRIFT measurements were performed in a Bio-Rad Digilab Division FTS-65A/896 spectrometer, taking 256 scans per sample with 4 cm^{-1} resolution. The samples were mixed with dry KBr (2 wt %), and pure dry KBr was used as reference.

UV−vis−DR spectra were recorded in a Unicam 8700 spectrometer using a Thermo-Electron RSA-UC 40 diffuse reflectance cell. The presented spectra are the average of three separate scans performed at a speed of 120 nm/min with a bandwith of 2 nm. The samples were mixed with dry KBr (2 wt %), and pure dry KBr was used as reference.

The specific surface area of the different samples was determined by the BET method from N_2 adsorption isotherms at 77 ± 0.5 K (Micromeritics Gemini 2375 surface area analyzer). Before the adsorption measurements, the samples were evacuated (1×10^{-5} mmHg) at 100 °C overnight.

Small-angle X-ray scattering was measured in a vacuum using $Cu_{K\alpha}$ radiation (Philips PW 1830 X-ray generator at a voltage of 50 kV, tube current of 40 mA, and wavelength of λ=0.154 nm). The powdered samples were placed in a sample holder with a thickness of 0.5 mm. The intensity of the scattered radiation was measured by a position sensitive detector (PDS 50M) controlled by ASA software in an angle range of $2\Theta = 0.05-8°$. Absorption intensities (A_s, A_b) were determined by the so-called moving slit method.[19] The $I(h)$ scattering function was normalized and corrected by the background scattering for determination of the structural parameters. The detailed calculation procedure is reported in the Appendix.

Morphology of the pure and phosphated titania was studied by a scanning electron microscope (SEM; Hitachi, S-4700).

Photo-oxidation of ethanol was performed in the reactor (volume of ca. 700 mL) at 25 ± 0.1 °C. The photoreactor consists of two concentrically positioned tubes, namely an inner quartz tube and an outer Pyrex glass tube. The light source of the reactor was a 15 W low pressure mercury lamp (GCL307T5L/CELL LightTech, Hungary) with a characteristic emission wavelength at $\lambda_{max} = 254$ nm. The catalyst was sprayed onto the outer side of the inner quartz tube from 30 (m/v) % aqueous dispersion using a N_2 stream. The surface of the catalyst film was 175.8 cm^2, and the catalyst mass per unit surface was 0.285 ± 0.045 mg/cm^2. The calculated thickness of the films was 0.86 μm ± 0.1 μm. Prior to catalytic test reactions, the films were conditioned by 1 h irradiation with UV−vis light at 80 °C followed by a 1 h vacuum pretreatment ($p = 1 \times 10^{-3}$ mm Hg). The reactor was filled with dry synthetic air ($[H_2O] < 5$ ppm) to a final pressure of 760 mm Hg. After delivery of ethanol and water, the system was left to stand for 30 min for evaporation of the components and establishment of the adsorption equilibrium. The reaction starts with switching on the UV lamp. Sampling from the gas phase (1 mL) was performed at selected time intervals, and the composition was analyzed in a gas chromatograph (Shimadzu GC-14B) equipped with a thermal conductivity detector (TCD). The temperature of the column (HayeSep Q, length 2 m) was 120 °C. A sample volume of 1 mL was introduced through a six-way valve to the on-line GC used for quantitative analysis of ethanol and CO_2. The initial concentration of ethanol was 12030 ppm at relative humidity of ~70%. The

(14) Bertóti, I.; Mohai, M.; Sullivan, J. L.; Saied, S. O. *Appl. Surf. Sci.* **1995**, *84*, 357.
(15) Bertóti, I.; Mohai, M.; Renevier, N. M.; Szilágyi, E. *Surf. Coat. Technol.* **2000**, *125*, 173.
(16) Mohai, M. *Surf. Interface Anal.* **2004**, *36*, 828.
(17) Evans, S.; Pritchard, R. G.; Thomas, J. M. J. *Electron Spectrosc. Relat. Phenom.* **1978**, *14*, 341.
(18) Reilman, R. F.; Msezane, A.; Mansor, S. T. *J. Electron Spectrosc. Relat. Phenom.* **1976**, *8* 389.
(19) Stabinger, H.; Kratky, O. *Makromol. Chem. Phys.* **1978**, *179* (6), 1655.

Table 1. Surface and Bulk Composition of Phosphate-Modified Titania Samples

Sample name	P/Ti atom ratio calculated	P/Ti atom ratio ICP−AES	P/Ti atom ratio XPS	$(P/Ti)_{XPS}$:$(P/Ti)_{ICP-AES}$
P−TiO_2/0.01	0.010	0.012	0.120	10
P−TiO_2/0.05	0.050	0.055	0.220	4
P−TiO_2/0.10	0.10	0.106	0.245	2.3

photocatalytic experiments were repeated three times and their reproducibility was better than 3%.

Results and Discussion

Composition and Chemical Structure. The results of the ICP-AES analysis (Table 1) show that P/Ti ratios are identical with those of the calculated ones. This means that the added amount of phosphoric acid reacted completely with the titania at the applied preparation conditions. In addition to the determination of the surface composition, XPS analysis was also extended to the evaluation of the chemical structure of the elements constituting the surface of the samples. For this, the position and shape of the best documented spectral lines, i.e., the O 1s, Ti 2p, P 2p, and C 1s (present as common surface carbon impurity), were recorded and studied. The ICP-AES analysis for total P/Ti ratios was supplemented with determination of surface P/Ti ratios determined by XPS, which are also included in Table 1. The surface P/Ti ratio was fond to be 10-, 4-, and 2.3-fold higher, respectively, than the total P/Ti. Comparison of the O 1s, Ti 2p, and P 2p spectral lines of the samples with those of the pure TiO_2 sample is depicted in Figure 1. The main Ti $2p_{3/2}$ components of the Ti 2p doublets at 459.0 eV (Figure 1a) are all narrow (full width is 1.55 eV) and symmetric, manifesting one single chemical state, representing O−Ti−O type chemical environment. Our results clearly contradict with that published for phosphated titania by Yu et al., who found a Ti $2p_{3/2}$ component at an unrealisticly high B.E. of 459.7 eV and assigned it to Ti ions in octahedral coordination with oxygen.[12] The O 1s spectrum at 529.9 ± 0.1 eV for the undoped TiO_2 (lowest curve in Figure 1b) is almost symmetric corresponding to the Ti−O−Ti state. The spectra of the P-doped samples are clearly asymmetric, having a low intensity shoulder on the high B.E. side. The energy position of this shoulder, as determined by a peak synthesis procedure, is at 530.8 ± 0.2 eV and related to oxygen in the P═O and Ti−O−P environments.[14] The atomic ratio of this oxygen to the corresponding P-content varied between 2.5 and 3, in accordance with the expected phosphate stoichiometry. This is in full agreement with the 0.8 eV shift between the Ti-bonded and P-bonded oxygens reported also for phosphated titania earlier.[12] Higher-energy, but lower-intensity, oxygen components at about 531.5 and 532.5 eV are assignable to O−H and O═C or C−O−C bonds, incorporated, at least partly, with the adventitious carbon contamination. The P 2p peaks for the P-doped samples (Figure 1c) are centered at 133.7 ± 0.2 eV, the value of which is characteristic for the phosphate state.[12]

The results of diffuse reflectance infrared Fourier transform spectroscopy (DRIFT) are presented in Figure 2. After phosphoric acid treatment on TiO_2, a new absorption peak appears in the range of 980−1200 cm^{-1}. These broad bands are associated with the characteristic stretching vibrations of PO_4 groups, and their intensities are proportional to phosphate content. The peak at 1630 cm^{-1} can be assigned to the bending mode of water. The broad band around 3400 cm^{-1} is assigned to the O−H stretching mode. The intensities of these bands also increase with phosphate content.

DRIFT spectra reveal that, in the course of phosphoric acid treatment of the TiO_2 suspension, PO_4^{3-} ions are bonded to the surface of titanium dioxide in amounts proportional to the phosphoric acid concentration applied. The surface OH groups of TiO_2 can react with phosphate ions, leading to cross-linking.[20] Connor and McQuillan also studied the

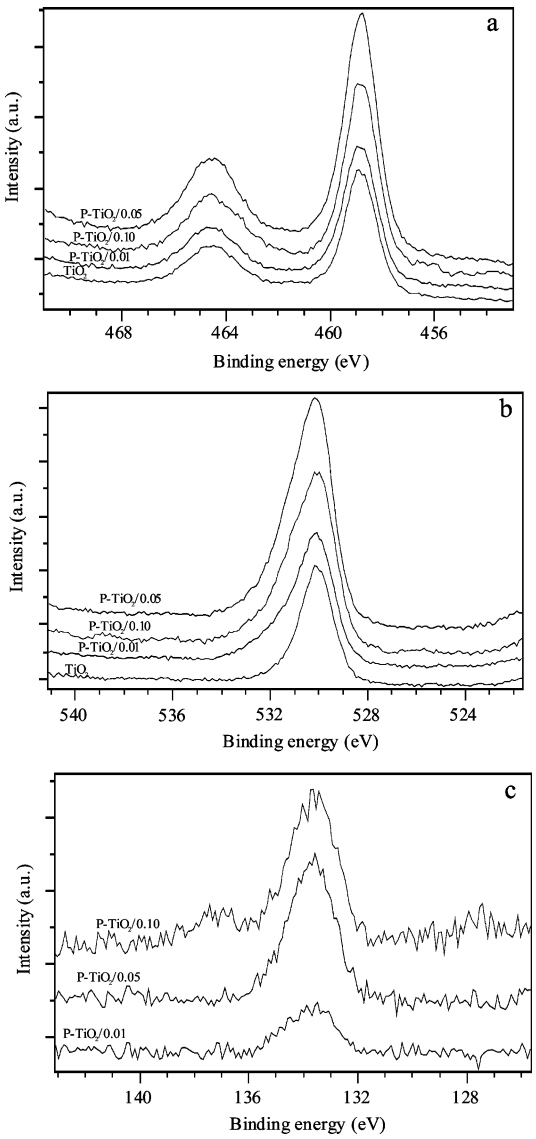

Figure 1. XPS spectra of the (a) Ti 2p, (b) O 1s, and (c) P 2p regions taken on pure and phosphate-modified titania samples.

(20) Ciesla, U.; Schacht, S.; Stucky, G. D.; Unger, K. K.; Schuth, F. *Angew. Chem., Int. Ed.* **1996**, *35*, 541.
(21) Connor, P. A.; McQuillan, A. J. *Langmuir* **1999**, *15* 2916.
(22) Gong, W. *Int. J. Miner. Process.* **2001**, *63*, 147.
(23) Beydoun, D.; Amal, R.; Low, G.; McEvoy, S. *J. Nanopart. Res.* **1999**, *1*, 439.

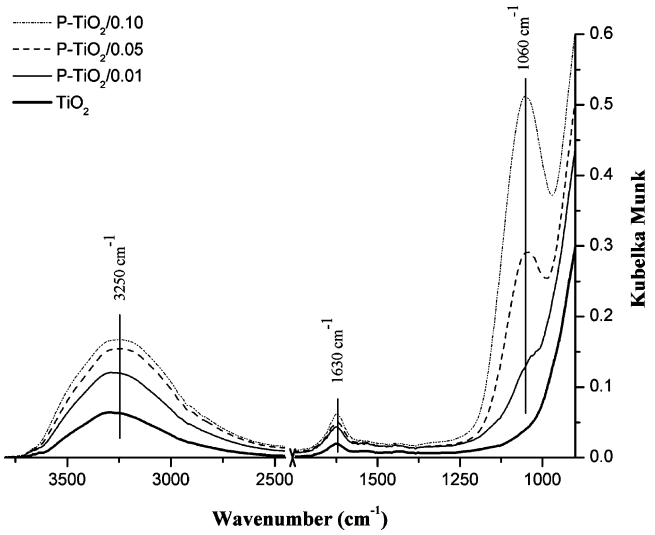

Figure 2. DRIFT spectra of pure and phosphate-modified titania samples.

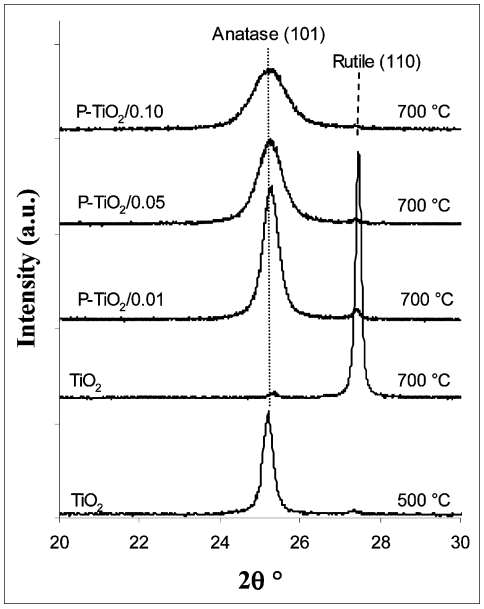

Figure 3. XRD patterns of the pure TiO_2 (calcined at 500 and 700 °C) and the phosphate-modified titania samples (calcined at 700 °C).

adsorption of orthophosphate on the surface of titanium dioxide from aqueous solution by in situ internal reflectance spectroscopy.[21] They reported strong binding of the bidentate form of phosphate to the surface. W. Gong identified two species on the surface, namely the bridging bidentate surface complex $(TiO)_2PO_2$ with C_{2v} symmetry and the electrostatically adsorbed PO_4^{3-} ion with T_d symmetry.[22]

Crystalline Structure and Porosity. Results of X-ray diffraction measurements also reveal significant changes upon increasing the phosphate content of titanium dioxide. Diffractograms of pure TiO_2 and P−TiO_2 samples with various phosphate contents are compared in Figure 3. It is clear that in the case of untreated TiO_2, the anatase → rutile transition (between 500 and 700 °C) brought about by heat treatment is nearly complete. Conversely, in the case of P−TiO_2/700 °C samples, the dominant phase is anatase (75−86 wt %). The half-widths of anatase (101) peaks increased with increasing phosphate content, indicating a decrease in crystallite size. The calculated crystal diameters are summarized in Table 2. The anatase crystal diameters in the

Table 2. Composition of Crystallite Phase and Particle Size of Pure and Different Phosphate-Modified Titania Samples Calcined at 700 °C

sample	anatase (wt %)	rutile (wt %)	*d* (nm)
TiO_2	<1	>99	>100
P−TiO_2/0.01	86	4	23.7
P−TiO_2 /0.05	82	2	11.9
P−TiO_2/0.10	75	<1	9.4

P−TiO_2/700 °C samples were in the range of 9.4−23.7 nm depending on phosphate content. The anatase content of the samples also decreases with increasing phosphate content. The data in the table clearly demonstrate that ∼10−25 wt % of the samples with high phosphate contents are amorphous (a mixture of amorphous titanium dioxide and amorphous titanium phosphate). It is obvious from the results that phosphate modification delays both the crystallization of anatase (the amorphous titania−anatase transition) and the anatase−rutile phase transformation (i.e., a higher temperature is needed).

For P−TiO_2/0.05 and P−TiO_2/0.10 samples calcined at 900 °C, titanium(IV) phosphate TiP_2O_7 with cubic lattice was identified (JPCDS 38-1468), which according to the evidence of XPS and ICP-AES measurements is accumulated in the surface region of the particles.

N_2 adsorption isotherms and BET surface areas calculated thereof are presented in panels a and b of Figure 4. Figure 4a demonstrates that the structure of pure titanium dioxide collapses after calcination at 700 °C. In contrast, hysteresis observed in the case of phosphated titanium dioxide samples is indicative of porous structure. The BJH pore size distribution curves (not shown) have a peak centered at about 3.3 nm for P−TiO_2/0.05 and 4.9 nm for P−TiO_2/0.10. The mesopores of the sample with the higher phosphate content are more monodisperse.

The specific surface area (a^s_{BET}) increases with increasing phosphate content at a given calcination temperature (Figure 4b) and for samples calcined at 700 °C are 10, 75, and 105 m^2/g at P/Ti atomic ratios of 0.01, 0.05, and 0.10, respectively, whereas a^s_{BET} for the unmodified rutile phase TiO_2 is 6 m^2/g.

The specific surface areas of the samples decrease with increasing calcination temperature. The higher the P/Ti ratio, the slighter this decreasing tendency. Thus, surface modification by phosphate enhanced the thermal stability of titanium dioxide.

The angle-dependence of the intensity of X-rays scattered from an ensemble of colloidal particles reflects the structural inhomogeneities of the dispersed system; thus, it carries information about the size and aggregation state of the particles, and the specific surface area and porosity of the material. The Porod plots of scattering curves of pure TiO_2 and the three phosphated samples (with P/Ti ratios of 0.01, 0.05, and 0.1) calcined at 500 °C are represented in Figure 5a. Porod plots of scattering curves of the P−TiO_2/0.05 sample calcined at 100, 500, and 900 °C are shown in Figure 5b.

The log−log scattering curves were analyzed for mass (D_m) fractal dimensions. D_m values varied systematically with increasing calcination temperature between 1.69 and 2.41, showing compactation of the particle structure. This tendency

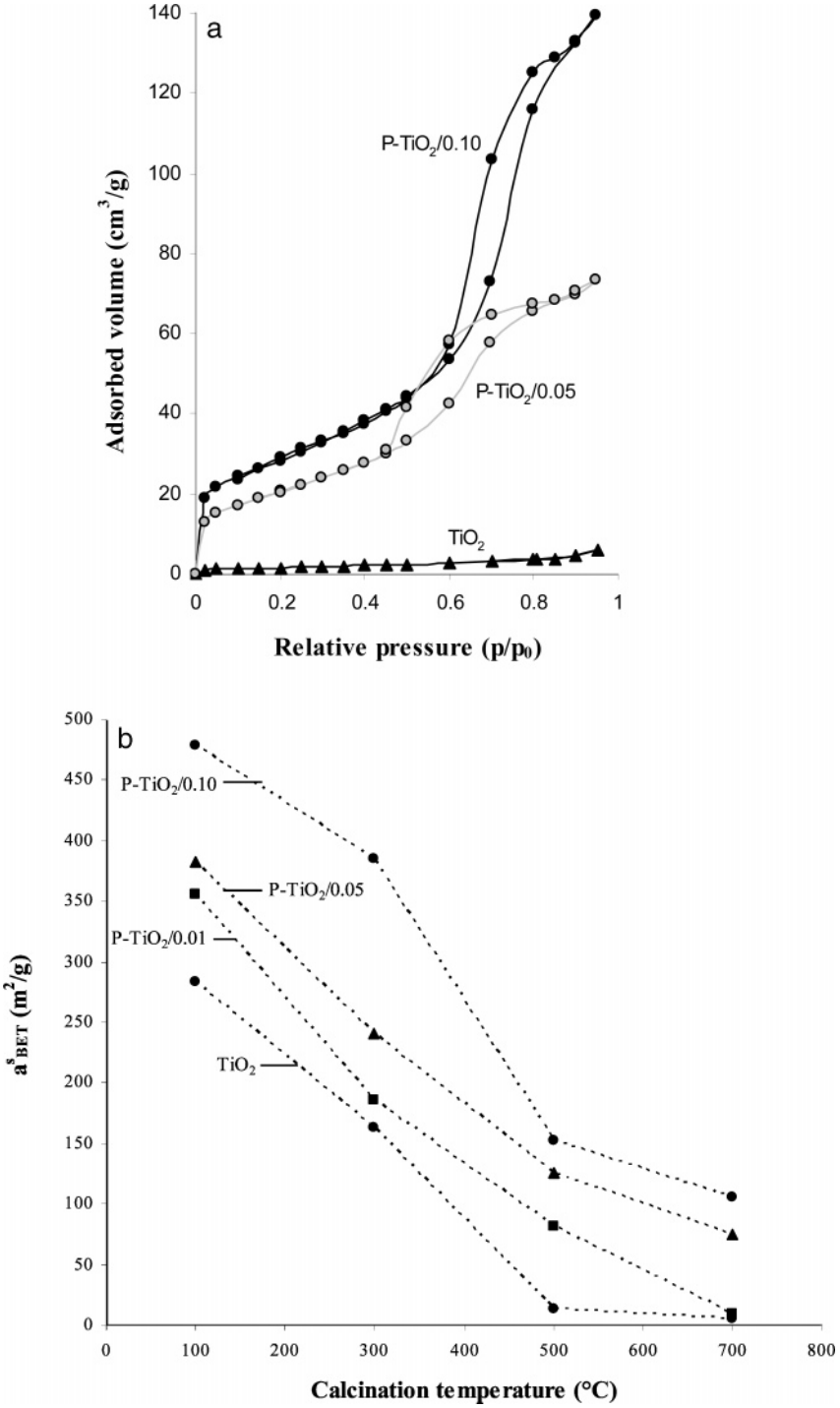

Figure 4. (a) Nitrogen adsorption−desorption isotherms of pure and two phosphate-modified titania samples calcined at 700 °C (b) Specific surface area of pure and phosphate-modified titania samples as a function of calcination temperature.

was less pronounced for the samples with increasing phosphate contents.

The specific surface areas of the samples were calculated from the Porod plots presented in panels a and b in Figure 5. The calculated parameters (the Porod constant K_p, the specific surface area S_P, the correlation length l_c, and the characteristic length of the solid-phase l_1) are given in Table 3. K_p values and S_p increased with phosphate content and decreased with temperature. Particle correlation lengths also changed in parallel with phosphate content and temperature. Thus, we can conclude that the increase in phosphate content leads to a decrease in particle size and a consequent increase in specific surface area. Results for specific surface areas from SAXS experiments correlate well (0.3−8.9% difference) with the data from BET determinations (Table 3). It is also observed that characteristic lengths (l_1) increased with increasing correlation lengths (l_c), showing the tendency of the structure to compact when calcination temperature is increased from 100 to 900 °C. Both correlation and characteristic lengths decreased with increasing phosphate content, in accordance with the increase in specific surface area.

Morphology. SEM images of different phosphate-modified titania samples calcined at 700 °C are presented in Figure 6. The P/Ti ratios of the samples determined by EDX analysis

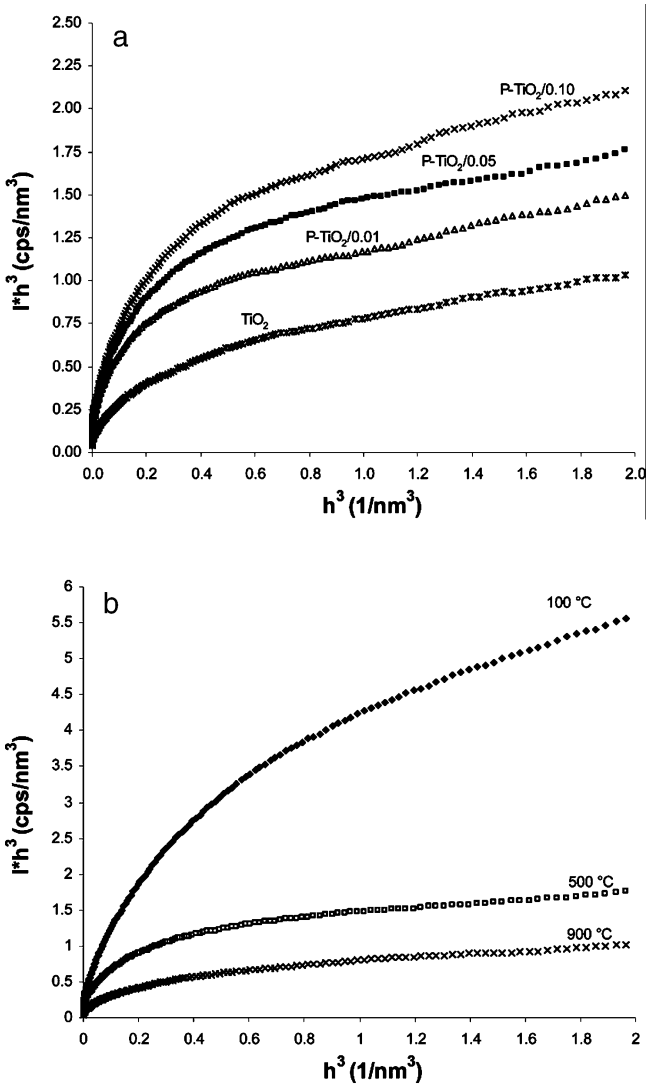

Figure 5. (a) X-ray scattering curves in Porod representation for pure and phosphate modified titania samples calcined at 500 °C (b) X-ray scattering curves in Porod representation of P−TiO_2/0.05 calcined at different temperatures.

Table 3. SAXS Parameters of Pure and Phosphate-Modified Titania Samples at Different Calcination Temperatures

sample name	T (°C)	K_p (cps/nm^3)	S_p (m^2/g)	l_c (nm)	l_1 (nm)	a^s_{BET} (m^2/g)
TiO_2	100	2.063	255	6.8	4.3	283
	500	0.589	34	41.6	40.7	14
	900	0.396	23	56.6	57.5	
P−TiO_2/0.01	100	1.989	345	5.0	3.3	356
	500	1.032	76	22.8	14.9	82
	900	0.641	39	47.0	39.3	
P−TiO_2/0.05	100	3.655	383	5.1	2.4	384
	500	1.259	102	17.0	11.1	131
	900	0.576	45	34.7	40.6	
P−TiO_2/0.10	100	5.955	438	5.0	1.9	477
	500	1.561	122	14.3	9.1	153
	900	0.617	43	35.3	44.3	

are 0.013, 0.048, and 0.100, in good agreement with the results of ICP-AES for samples P−TiO_2/0.01, P−TiO_2/0.05, and P−TiO_2/0.10, respectively. The size of primary particles decreased with increasing phosphate content and their monodispersity increased. Average particle diameters at atomic ratios of P/Ti = 0.01, 0.05, and 0.10 are 25, 11, and 10 nm, respectively. Average particle sizes are in good agreement with those calculated by the Scherrer equation:

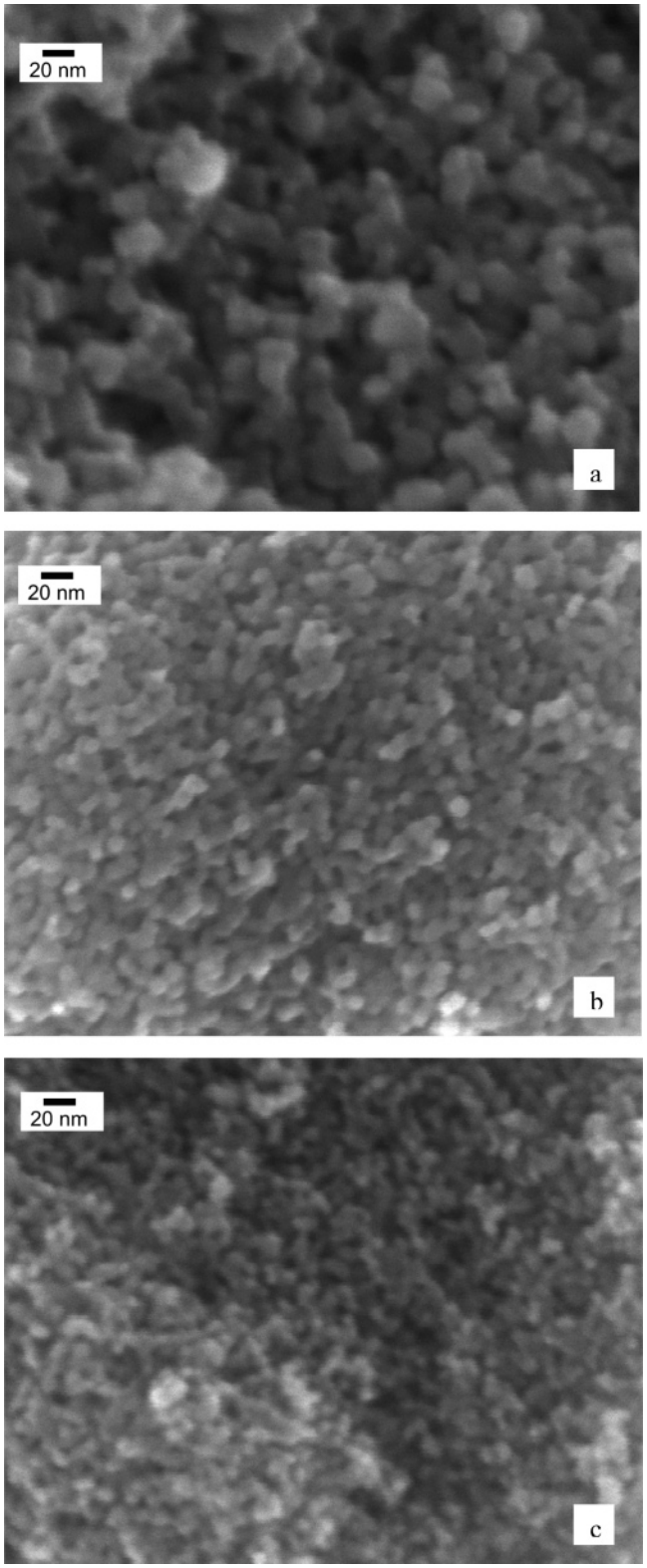

Figure 6. SEM picture of (a) P−TiO_2/0.01, (b) P−TiO_2/0.05, and (c) P−TiO_2/0.10 calcined at 700 °C.

the difference between values determined by the two methods is less than 5%. Because of the high-temperature heat treatment, however, aggregates in the micrometer range can be observed in a wide range of particle sizes. No significant difference could be observed in particle morphology: the primary particles were spherical regardless of their phosphate content.

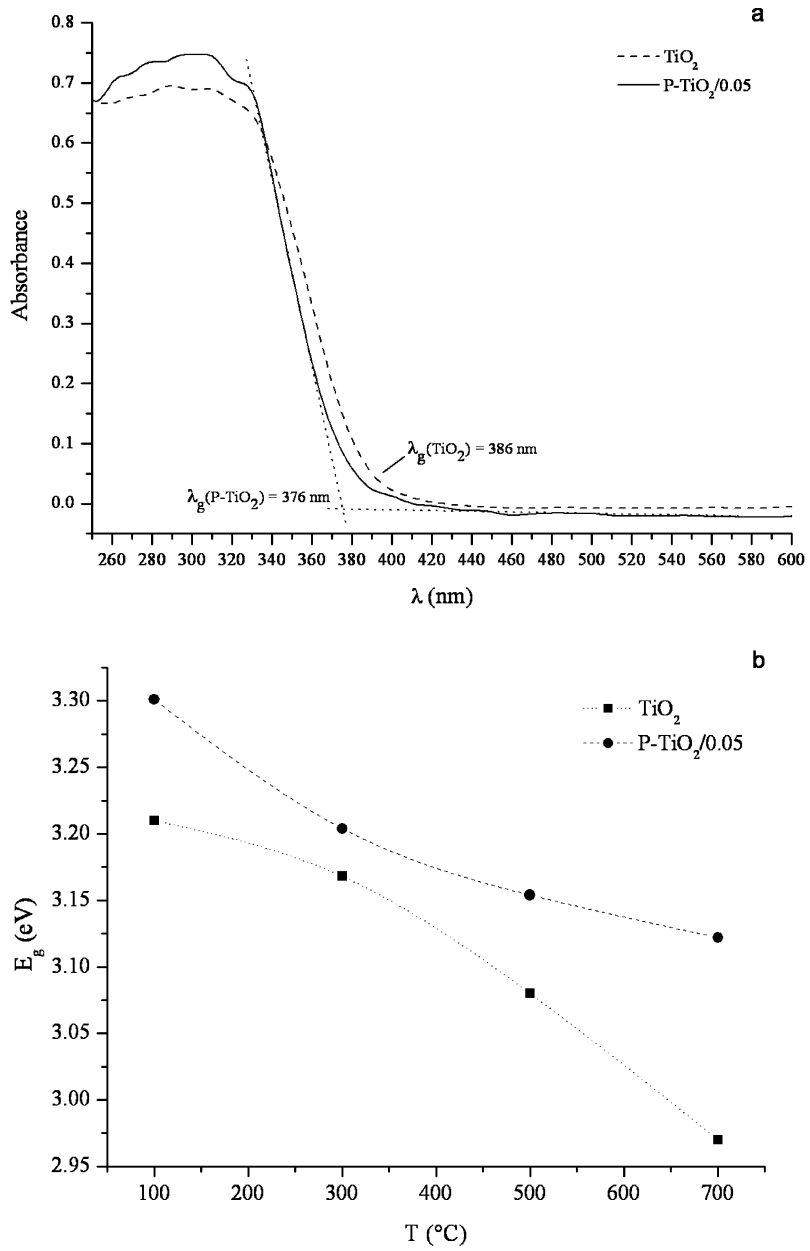

Figure 7. (a) Diffuse reflectance UV−vis spectra of TiO_2 and P−TiO_2/0.05 dried at 100 °C; (b) band gap energy of TiO_2 and P−TiO_2/0.05 as a function of calcination temperature.

Optical Band Gap. The diffuse reflectance UV−vis spectra of TiO_2 and P−TiO_2/0.05 samples are compared in Figure 7a. It can be observed that the adsorption edge is shifted to shorter wavelength after phosphoric acid treatment on titania. A similar blue shift was observed by Colón et al. in the case of phosphoric acid pretreatment of titanium dioxide.[11] Band gap energies (E_g) determined from the absorption edge are summarized in Figure 7b. As can be seen in Figure 7b, the E_g of phosphate-modified titania exceeds E_g of pure TiO_2 at each calcination temperature. The higher band gap energy of P−TiO_2 is partly accounted for the change in the structure of the titanium dioxide surface (chemisorbed phosphate) and partly for the smaller particle size of TiO_2 (quantum-size effect[23]).

Band gap energy decreased with increasing calcination temperature in the case of pure and phosphate-modified titania; however, it was less significant in the case of P−TiO_2 samples. The red shift observed in the course of calcination may be due partly to increasing particle size of anatase and partly to the anatase−rutile phase transition (between 500 and 700 °C).

Photocatalysis. The activities of the phosphate-modified titania samples calcined at 700 °C were compared in the gas-phase catalytic degradation of ethanol at 25 °C. Two main intermediates of ethanol oxidation were identified (acetaldehyde, formaldehyde), whose quantitative analysis is not included in this publication. CO_2 formation was not detectable in the absence of catalyst within the time frame of irradiation.

The catalytic activities of the phosphate-modified samples were compared to Degussa P25 TiO_2, an excellent and well-known photocatalyst that has been extensively studied in the degradation of volatile organic compounds.[24] The lowest conversion was observed on the sample with the lowest

(24) Mills, A.; Le Hunte, S. *J. Photochem. Photobiol., A* **1997**, *108*, 1.

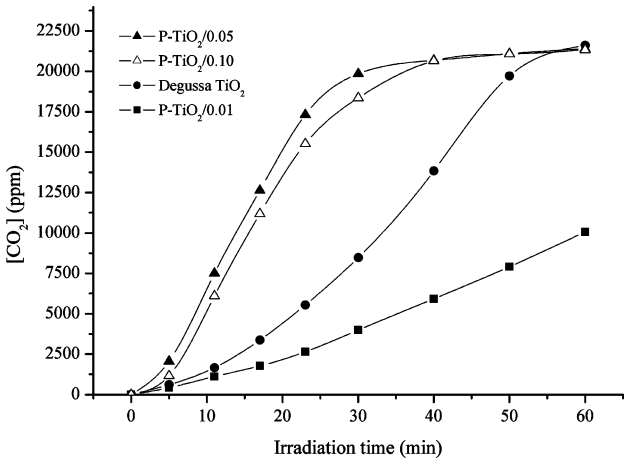

Figure 8. Evolution of CO_2 on Degussa P25 and different phosphate-modified titania samples (calcined at 700 °C) as a function UV irradiation time.

phosphate content (P−TiO_2/0.01) (Figure 8.). Total oxidation of ethanol is completed much faster on samples P−TiO_2/0.05 and P−TiO_2/0.10 than on Degussa P25. When the phosphate content increased from P/Ti = 0.05 to 0.10, the rate of photooxidation is not increased further; indeed, a slight decrease was observed.

Comparison of the structural parameters of samples P−TiO_2/0.10 and P−TiO_2/0.05 reveals that the specific surface area of sample P−TiO_2/0.10 is 40% larger, whereas its anatase content is 7 wt % lower than the corresponding values of sample P−TiO_2/0.05. Although higher phosphate contents allow the preparation of samples with larger specific surface areas, because of their decreased anatase contents, these may have lower photoactivities. It is therefore not expedient to increase the P/Ti atomic ratio to >0.10. The sample P−TiO_2/0.01 has a high anatase content (86%) but a low specific surface area (10 m^2/g), which also decreases the reaction rate. It follows that, in the course of preparation, phosphate content has to be optimized in a way to attain the largest possible specific surface area at the highest possible anatase content.

In addition to the effect of phosphate modification on the structure of titanium dioxide, we also examined how surface-bound phosphate affects the rate of the oxidation of ethanol. To this end, we removed phosphate groups from the surface of the most active P−TiO_2/0.05 sample by treatment with $NaHCO_3$ solution. After the hydrogen carbonate treatment, the phosphorus/titanium ratio of the surface decreased from 0.22 to 0.032 (on the basis of XPS measurements), whereas the main structural parameters of titanium dioxide (anatase content, particle size, specific surface area) were not altered by dephosphatation.

As demonstrated by Figure 9, the oxidation of ethanol is significantly slower on titanium dioxide with dephosphated surface: in 30 min, only 14% of the initial amount of ethanol was converted to carbon dioxide, whereas in the case of the phosphate-modified sample, conversion was 84%. According to our X-ray measurements the anatase content and the crystal size of the dephosphated sample were not modified by $NaHCO_3$ treatment. It follows that the phosphate groups bound on the surface of TiO_2 are responsible for the rapid photooxidation taking place on the P−TiO_2 samples.

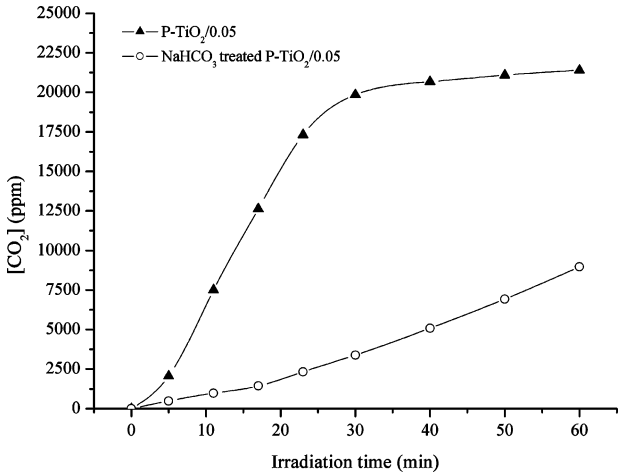

Figure 9. Evolution of CO_2 on P−TiO_2/0.05 and $NaHCO_3$-treated P−TiO_2/0.05 samples (calcined at 700 °C) as a function UV irradiation time.

On the one hand, phosphate ions incorporated into the surface of TiO_2 may inhibit the electron−hole recombination because of their ability to trap photogenerated holes. On the other hand, they are capable of converting reactive radicals by the photogenerated holes, which may later react with the adsorbed organic compounds. Trapping of photogenerated holes via the formation of reactive radicals may result in improved photooxidation.[25]

Thus, the presence of phosphate has a complex effect on the photocatalytic activity of the samples: on the one hand, it regulates their structural properties (anatase content, particle size, specific surface area); on the other hand, the surface-bound phosphate may improve the charge separation and inhibit the charge carrier recombination. The latter is essential in improving the overall quantum efficiency for interfacial charge transfer.[26]

Conclusion

Phosphate-modified titanium dioxide samples were prepared by phosphoric acid treatment of amorphous titania. It was shown that the phosphoric acid treatment of TiO_2 increased the thermal stability of the samples and hindered compaction and sintering of the nanosized TiO_2 particles. Surface-bound phosphate profoundly affects the crystallization of titania: it delays the formation of the anatase phase and crystallite growth and inhibits the anatase−rutile phase transformation.

Vapor-phase photo-oxidation of ethanol was significantly faster on the P−TiO_2 samples with optimal phosphate content than on Degussa P25. It is proposed that surface-bound phosphate has a complex effect on the photooxidation of ethanol. On the one hand, it affects formation of photoactive anatase content and helps to preserve the high specific surface area of the samples. On the other hand, phosphate modification of the TiO_2 surface may promote the photo-oxidation of ethanol by enhancing charge separation.

Appendix

The specific surface area and fractal dimension has been evaluated by the analysis of small-angle X-ray scattering

(25) Carp, O.; Huisman, C. L.; Reller, A. *Prog. Solid State Chem.* **2004**, *32*, 33.
(26) Bedja, I.; Kamat, P. V. *J. Phys. Chem.* **1995**, *99*, 9182.

curves.[27,28] The surface area per unit volume of the sample was calculated by the equations

$$\frac{S}{V} = \pi \frac{\lim_{h \to \infty} I(h)\, h^4}{\int_0^\infty h^2\, I(h) dh} \tag{1}$$

and

$$a^s_{SAXS} = \frac{(S/V) \times 10^3}{d} \tag{2}$$

where h is the scattering vector, S/V is the specific surface area of the particles (relative to the unit volume V; nm^2/nm^3), and d is the density of the powder (g/cm^3). The intensity of the scattered radiation I is the function of the scattering vector

$$I(h) = \eta^2(0) V \int_0^\infty 4\pi r^2 \gamma_0(r) \frac{\sin hr}{hr} dr \tag{3}$$

where $\eta^2(0)$ is the function of the electron density fluctuation $\eta(r) = (\rho_e(r) - \rho_e)$ in the scattering volume V

$$\eta^2(0) = \frac{1}{V} \int_0^\infty (\rho_e(r) - \rho_e)^2 d^3 r \tag{4}$$

and $\gamma_0(r)$ is the correlation function given by

$$\gamma_0(r) = \frac{\eta^2(r)}{\eta^2(0)} \tag{5}$$

The specific surface area of the particles S/V (eq 1) was calculated from the Porod region of the scattering function, for which the following relationship holds[29−31]

$$I(h) = \eta^2(0) 2\pi \frac{S}{h^4} \tag{6}$$

S/V is then given by eq 1, through calculating the Porod constant K_P

$$K_P = \lim_{h \to \infty} I(h)\, h^4 \tag{7}$$

for the case of a desmeared beam and

$$K_P = \lim_{h \to \infty} I(h)\, h^3 \tag{8}$$

for no desmearing, and through calculating the invariant Q

$$Q = \int_0^\infty h^2\, I(h)\, dh \tag{9}$$

for the case of the desmeared beam, or the first momentum M_1

$$M_1 = \int_0^\infty h\, I(h)\, dh \tag{10}$$

in the case of no desmearing.

The correlation length l_c, a property of the porous system characterizing the statistical distribution of inhomogeneities, has been calculated from S/V and thw volume fractions data w_1 and w_2 of the solid and gas phases, respectively. The relationship defined by Porod has been used[27,30]

$$\frac{S}{V} = \frac{8 w_1 w_2}{l_c} \tag{11}$$

and the characteristic length values l_1 and l_2 for the two phases separately were calculated by[32]

$$l_1 = \frac{4 w_1}{S/V} \, l_2 = \frac{4 w_2}{S/V} \tag{12}$$

The fractal dimensions are given by the slope of the middle section of the log $I(h)$ − log h scattering functions. The surface fractal and the mass fractal dimensions have been calculated by D_s = slope + 5 and D_m = slope + 1, respectively.[33]

CM070692R

(27) Glatter, O.; Kratky, O. *Small-Angle X-ray Scattering*; Academic Press: New York, 1982.
(28) Kriechbaum, M.; Degovics, D.; Tritthardt, J. *Prog. Colloid Polym. Sci.* **1989**, *79*, 101.
(29) Porod, G. *Kolloid Z.* **1951**, *124*, 83.
(30) Porod, G. *Kolloid Z.* **1952**, *125* 1.
(31) Kratky, O. *Angew. Chem.* **1960**, *72*, 467.
(32) Janosi, A. *Monatsch. Chem.* **1993**, *124*, 815.
(33) Dabrowsky, A.; Leboda, R.; Goworek, J.; Garbacz, J. K. Characterization of inorganic adsorbents by means of adsorption at the liquid-solid interface. In *Adsorption on New and Modified Inorganic Adsorbents*; Studies in Surface Science and Catalysis 99; Dabrowsky, A., Tertykh, V. A., Eds.; Elsevier: Amsterdam, 1996; pp 649−672.